# Non-Isothermal Nucleation and Crystallization of 12-Hydroxystearic Acid in Vegetable Oils

**ARTICLE** *in* CRYSTAL GROWTH & DESIGN · NOVEMBER 2008

Impact Factor: 4.89 · DOI: 10.1021/cg8008927



**2 AUTHORS:**

Michael A Rogers
University of Guelph
**64** PUBLICATIONS **1,057** CITATIONS
SEE PROFILE

Alejandro Gregorio Marangoni
University of Guelph
**338** PUBLICATIONS **6,820** CITATIONS
SEE PROFILE

Article

# Non-Isothermal Nucleation and Crystallization of 12-Hydroxystearic Acid in Vegetable Oils

Michael A. Rogers, and Alejandro G. Marangoni

*Cryst. Growth Des.*, **2008**, 8 (12), 4596-4601 • DOI: 10.1021/cg8008927 • Publication Date (Web): 08 November 2008



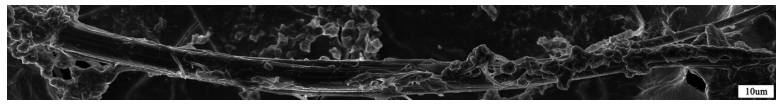

CRYSTAL GROWTH & DESIGN
2008
VOL. 8, NO. 12
4596–4601

# Non-Isothermal Nucleation and Crystallization of 12-Hydroxystearic Acid in Vegetable Oils

Michael A. Rogers*,† and Alejandro G. Marangoni‡

*Department of Food and Bioproduct Sciences, University of Saskatchewan, Saskatoon, Saskatchewan, Canada S7N5E2, and Department of Food Science, University of Guelph, Guelph, Ontraio, Canada N1G2W1*

*Received August 15, 2008*

**ABSTRACT:** The non-isothermal nucleation rate of a self-assembling fibrillar network of 12-hydroxystearic acid in canola oil was found to be inversely proportional to the undercooling time exposure of the system. Moreover, fiber growth kinetics could be adequately modeled using the Avrami equation. Both nucleation and fiber growth kinetics displayed two distinct regimes, above and below 5 °C/min. The abrupt change in the rate of nucleation, crystal growth rate constant, and the degree of branching at this cooling rate are related to whether the nucleation and crystal growth processes are governed by mass transfer or thermodynamics. At rapid cooling rates, above 5 °C/min, the driving force for both nucleation and crystal growth is the time-dependent chemical potential difference between the molten solid in solution and the crystallized solid (the degree of undercooling or supersaturation). At low cooling rates, however, the rate of crystallization is no longer determined by this dynamic chemical potential difference, but rather only limited by time. In the slow cooling regime, we show that there are no noncrystallographic mismatches which would lead to fiber branching. Using the models developed and adapted in this work, we could accurately predict the fiber length, rate of nucleation, rate of crystal growth, induction time of nucleation, and the degree of branching of a 12HSA SAFIN.

## Introduction

Organogels are finding many novel uses in the food, pharmaceutical, cosmetic and petrochemical industries, leading to renewed interest in these systems. This is in part due to their large diversity in terms of the possible microscopic and mesoscopic structures, which in turn leads to interesting and varied macroscopic functionalities.[1] In the food industry, organogels have the potential to minimize oil migration in multicomponent foods, such as cream-filled chocolates, and to provide structure to edible oils, thereby reducing the need for saturated and trans fatty acids. Organogels are being investigated for topical applications in drug delivery as well.[2] In this case, the rate of delivery is governed by the mesh size distribution within a gel and therefore understanding the nanostructure is of utmost importance.[3]

During the industrial manufacture of organogels, crystallization takes place under nonisothermal conditions where the temperature is changing as the material crystallizes. It has been shown that the crystallization behavior and structure of organogels is sensitive to both heat and mass transfer conditions, and that this in turn affects mechanical strength and oil binding capacity.[4] The nucleation behavior of these materials, in particular, is of great importance because it strongly affects structural features such as crystallite number, size and morphology, and the spatial distribution of mass.[5]

The nucleation process for 12HSA requires highly specific interactions to induce preferential one-dimensional growth. This one-dimensional growth results in fiber formation which may be described as "crystal-like".[6] The aggregation of the gelator molecules builds the primary structures (rods, tubes, or sheets) via noncovalent bonds, which in turn associate to create a three-dimensional network structure (secondary structure) via noncovalent interactions including hydrogen bonding, van der Waals interactions, $\pi-\pi$ stacking, and metal coordination bonds[7] Depending on how 12HSA−canola oil gels are produced, their microstructure can vary from a random highly branched network to a highly ordered network with less branching.[4,8] Each type of network has very different physical properties (i.e., macroscopic hardness, oil binding capacity, and degree of crystallinity).[4,8] Much work has been carried out on the isothermal nucleation and crystallization of organogels.[9−12] There is a general consensus among these authors that self-assembled fibrillar networks form via a nucleation−growth−noncrystallographic branching mechanism.[9−12] However, very little to no information exists on the nonisothermal nucleation and growth behavior of organogels.

Thus far, the potential of organogels as novel soft materials has been underutilized, on account of the inability to modify or predict the microstructure of the fibular network.[13] Furthermore, organogel stability is not well-understood. Alterations in concentration, storage temperature, and cooling rate can alter the network's ability to retain oil and affect the crystallinity of the supramolecular network. Thus, it is the purpose of this study to examine how 12 hydroxystearic acid (12HSA) crystals in vegetable oil are affected by nonisothermal crystallization conditions, specifically, the effects of cooling rate and annealing temperature on nucleation behavior, fiber growth, and crystal morphology.

## Methods

**Sample Preparation.** Ninety-nine percent pure DL-12HSA was obtained from Sigma-Aldrich (Catalogue no. 219967, St. Louis, MO) and the peak melting temperature determined to be 76 °C by differential scanning calorimetry (Q2000, TA Instruments, New Castle, DE, data not shown). Canola oil was obtained from Sunfresh Limited (Toronto, ON) and used as received. Two weight percent samples of 12HSA in canola oil were prepared by heating the 12HSA in canola oil to 85 °C for 30 min.

**Bright-Field Light Micrscopy.** Samples for thin film microscopy were removed from the oven at 80 °C and were placed on a 25 × 75 mm × 1 mm glass slide (Fisher Scientific, Pittsburgh, PA). No coverslip was used to attempt to prevent surface effects from a constrained

* Corresponding author. E-mail: michael.rogers@usask.ca. Tel: (306) 966 5028. Fax: (306) 966 8898.
† University of Saskatchewan.
‡ University of Guelph.

10.1021/cg8008927 CCC: $40.75 
Published on Web 11/08/2008

environment. The slide was then transferred into a thermostatically (80 °C) controlled microscope stage (Model LTS 350, Linkam Scientific, Surry, U.K.) and were cooled at 1−15 °C/min to 5 °C. Images were obtained using an Olympus BH polarized light microscope (Olympus, Tokyo, Japan) and a Sony XC-75 CCD video camera (Sony Corporation, Tokyo, Japan). Images were acquired using Scion Image Software (Scion Corporation, Fredrick, MD) and a 16-frame averaging method which resulted in an 8-bit grayscale image with a spatial resolution of 640 × 480 pixels. A 40× magnification objective lens with a 0.25 numerical aperture was used (Olympus, Tokyo). Image J was used for the analysis of the fiber radius and the number of crystals. Images were taken every 30 s during nucleation and crystal growth and the numbers of individual nuclei were counted on each micrograph in triplicate. During crystal growth, the length of the fiber was measured using Image J (Bethesda, MD).

**Fourier Transform Infrared Spectroscopy.** Two percent HSA/mineral oil (Fisher Scientific, NJ) was used for Infrared (IR) measurements because the carbonyl and hydroxyl singnals interfered with the measurement of the 12HSA signal making it to difficult to see changes in the spectra. Sodium sulfate anhydrous (Fisher Scientific) was added to ensure all the water was remove from the mineral oil as to not interfere with the hydroxyl signal. Infrared measurements were carried out on a Nicolet 20DXC IR Interferometer (Madison, WI) using a liquid-nitrogen-cooled MCT-B detector. To maintain the temperature, we cooled a glass cell with a water jacket at 1 °C/min and held it there for 15 min before measurements were taken at each temperature; the glass cell was mounted on a Teflon base containing a ZnSe hemispherical prism in an ATR configuration. The temperature of the sample was monitored using a thermocouple at the surface for the ZnSe prism. Five thousand scans were collected at a resolution of 4 $cm^{-1}$.

**Differential Scanning Calorimetry.** Samples of 2% HSA−canola oil and 2% HSA−mineral oil were melted at 80 °C and a drop of sol ranging from 10 to 12 mg was placed in an Alod-Al hermetic DSC pans. The sample and the pan were then heated for 30 min at 80 °C and stored for 24 h. The DSC chamber (Q2000, TA instruments, New Castle, DE) was precooled to the storage temperature before loading the sample was and the chamber continually flushed with nitrogen (0.5 mL/min). The samples were heated at 2 °C/min to determine the transition peak melting temperatures.

**Modeling Non-Isothermal Nucleation Kinetics.** Non-isothermal interpretation: Under nonisothermal conditions, the supersaturation, or supercooling, of the system is a dynamic quantity since the degree of undercooling ($\Delta T$) is changing in time as the material crystallizes. Marangoni et al. defined a supercooling-time parameter which is the effective exposure of the system to the supercooling until the initiation of nucleation.[14] This is calculated as the area under the supercooling-time trajectory from the time when the sample crosses the thermodynamic melting point, $T_m$, to the time where the first crystal nuclei appear ($t_c$) at the temperature of crystallization ($T_c$). This supercooling-time exposure ($\beta$) at nucleation can thus be defined as

$$\beta = \frac{1}{2}\Delta T_c t_c \tag{1}$$

Because the cooling rate is defined as $\varphi = \Delta T/\Delta t$ and at $T_c$, $t = t_c$ and $t_0 = 0$, then $\phi = \Delta T_c/t_c$. Substituting $t_c$ for $\Delta T_c/\varphi$ leads to an expression for the supercooling-time exposure at nucleation

$$\beta = \frac{1}{2}\frac{(\Delta T_c)^2}{\phi} \tag{2}$$

It is imperative to realize that a parametrization of the data relative to temperature and time is required for a proper description of the phenomenon of nucleation under nonisothermal conditions. Both the degree of supercooling at nucleation and the nonisothermal nucleation induction time are included in the parameter $\beta$. For our system, we found a linear dependence of the nucleation rate to the supercooling-time exposure, namely

$$J = J_{max} - s\beta \tag{3}$$

Using this model, it also possible to determine the energy required to initiate the nucleation process, possibly the energy of activation for nucleation. From $T_m$ to $T_c$, the onset of the phase transformation, no phase change has taken place. Thus, strictly specific heat has been removed from the system ($Q_m = C_p\Delta T$), where $Q_m$ is the heat removed from the system upon cooling per gram of material, $C_p$ is the specific heat (heat capacity), which for vegetable oils is ∼2.0 J $g^{-1}$ $K^{-1}$ in this temperature range. Substituting $Q_m/C_p$ for $\Delta T$ in eq 2, and substitution into equation 3, leads to the expression

$$J = J_{max} - \frac{sQ_m^2}{2C_p^2\phi} = J_{max} - \frac{\Psi}{\phi} \tag{4}$$

where $Q_m$ is proposed here to possibly represent the energy of activation for nucleation per unit mass (J/g). This quantity can then be multiplied by the average molecular weight of the 12HSA to obtain the molar energy of activation for nucleation. Therefore, from knowledge of slopes ($s$ and $\psi$) obtained from the linear regressions of eqs 3 and 4 to the data, the energy of activation for nucleation (J/g) would be calculated as

$$Q_m = C_p\sqrt{\frac{2\Psi}{s}} \tag{5}$$

## Results and Discussion

**Nucleation Kinetics.** The crystallization behavior of 12-hydroxystearic acid (12HSA), and therefore the structure of organogels structured by 12HSA, is sensitive to cooling rate.[4] Increased cooling rates lead to higher rates of nucleation, which in turn results in a decrease in crystal size and an increase in the number of nuclei (Figure 1). Figure 1 shows the 12HSA−canola oil melt cooled at 10 °C/min (left column), 5 °C/min (center column) and 1 °C/min (right column). Lower onset temperatures of nucleation were observed at higher cooling rates, indicating a higher degree of undercooling at the moment of nucleation, thus leading to the creation of a larger number of smaller crystals.[15] To quantify the nucleation process, we counted the number of independent crystals ($N$) on each micrograph and plotted them as a function of time ($t$) for each cooling rate (panels A and B in Figure 2). We then determined the first derivative of the $N$ vs $t$ curve, which corresponds to the nucleation rate. For further analysis, peak nucleation rate was used ($J_p$) (panels C and D in Figure 2). This method was developed to examine the nonisothermal nucleation process of triacylglyceride (TAG) melts.[14] Armed with an accurate measure of the rate of nucleation, we could investigate its dependence on cooling rate. A simple inverse relationship between the rate of nucleation and the cooling rate was found (eq 3). Interestingly, for triacylglycerides this dependence was exponential in nature. Hence, here we show that there is a difference between the nucleation processes of lipids and SAFiNs. One-dimensional fiber formation has been reported to be significantly different from triacylgylceride crystallization, where macroscopic phase separation occurs. In contrast, for SAFiNs, microscopic phase separation has been reported to occur.[6]

Examining the relationship between $J_p$ and cooling rate (Figure 1E), we noticed two distinct regimes with differing sensitivities to changes in cooling rate. At low cooling rates (i.e., less than 5 °C/min), nucleation rate did not change much as a function of cooling rate; however, above 5 °C/min, a much greater dependence of the rate of nucleation to the cooling rate was observed. The peak nucleation rate versus the supercooling time exposure parameter plot also shows two very distinct regimes (Figure 3). The rate of nucleation for rapidly cooled samples was a strong function of the supercooling time exposure ($p < 0.05$), whereas at low cooling rates, nucleation rate was not a function this supercooling time exposure ($p > 0.05$). This would suggest that at rapid cooling rates a time-dependent thermodynamic driving force controls the rate of nucleation. At slow cooling rates (i.e., <2.5 °C/min), the nucleation behavior did not show this dependence.

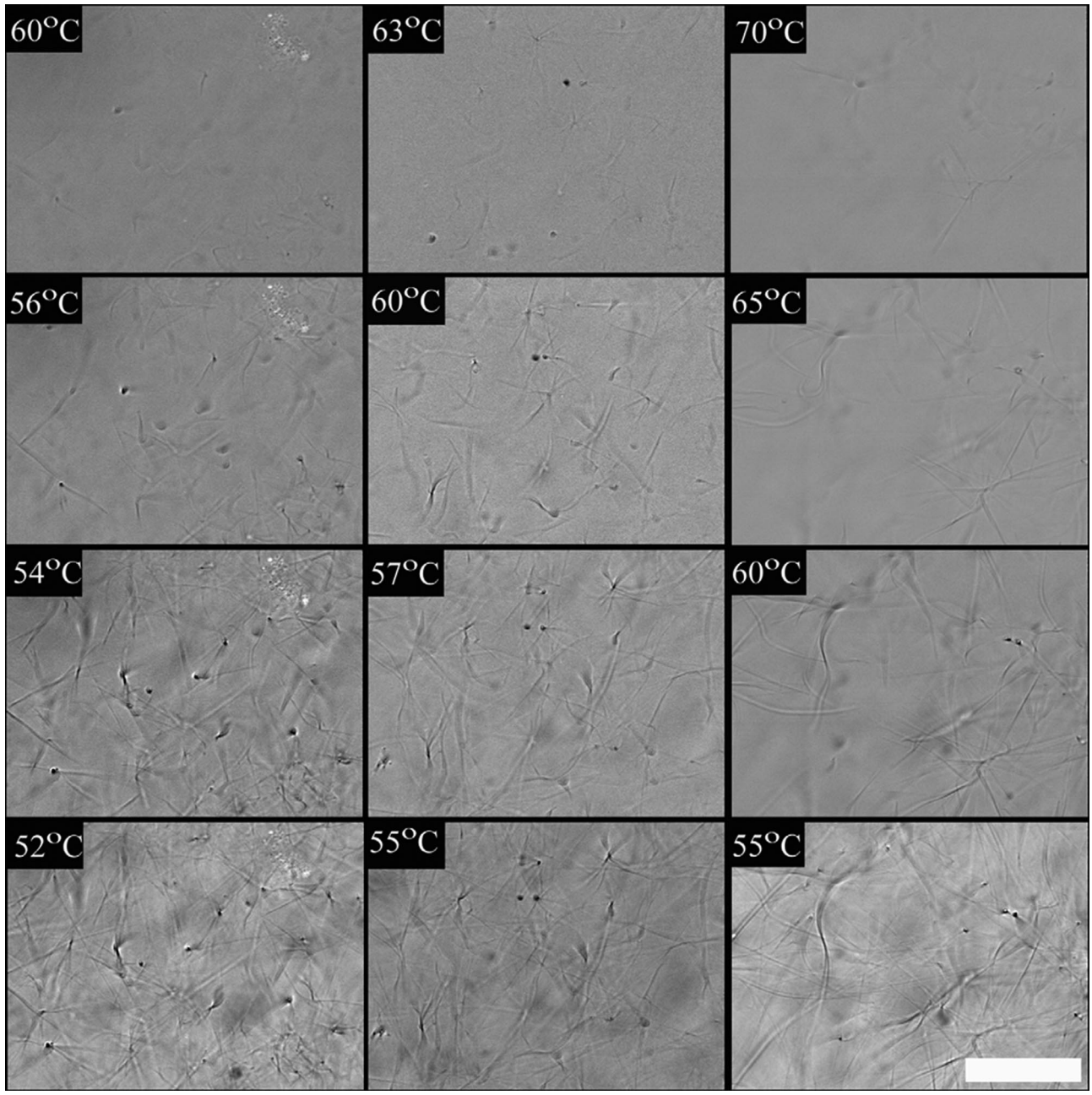


**Figure 1.** Brightfield images of 2 wt % HSA/canola oil gels during cooling at 10 °C/min (left), 5 °C/min (center), and 1 °C/min (right). Magnification bar = 100 $\mu$m.

Using eqs 3 and 4 and the slopes obtained from Figures 2E and 3, we can calculate the molar energy of activation for nucleation. For 12HSA (MW = 300 g/mol), we determined the energy of activation for nucleation to be 12.1 kJ/mol. This was an interesting finding since, on average, the energy of activation for nonisothermal triacylglycerol (TAG) nucleation was determined to be 39 kJ/mol,[14] which is five times greater than 12HSA nucleation. The difference between these two crystallization processes has been proposed to be due to macroscopic vs microscopic nucleation events.[16,17] Previous work suggests that microscopic phase separation (i.e., SAFiN nucleation) has a significantly lower energy of activation than macroscopic phase separation. This could be attributed to the ease of formation of a SAFiN nucleus. In our case, strong hydrogen bonding between 12HSA molecules in the melt would greatly increase the probability for the formation of a stable nucleus. This would result is a smaller critical radius for nucleation because of the increased stability of the embryo. This, in turn would decrease the magnitude of the area-related free energy term in the Fisher−Turnbull model. Ultimately, this leads to a decrease in the free energy of activation for nucleation. In contrast, a much larger embryo must be formed during TAG nucleation because of the relatively weak and nonspecific interactions between TAGs, which makes it more difficult to form a stable embryo capable of growing into a crystal.

Using the argument of microscopic phase separation, there should be significant hydrogen bonding in the melt. Fourier transform infrared spectroscopy (FTIR) was used to probe if hydrogen bonding was present between the hydroxyl and/or the carbonyl groups in the melt (Figure 4). Figure 4A shows the presence of the hydrogen bonding between the hydroxyl groups with an absorbance band at approximately 3200 $cm^{-1}$. Figure 4B indicates the presence of both the non-hydrogen bond carbonyl group at 1710 $cm^{-1}$ and the hydrogen-bonded carbonyl group at 1700 $cm^{-1}$ (Figure 4B). We can see that the 12HSA−mineral oil gel melts at 54.4 °C (Figure 4D, solid line),

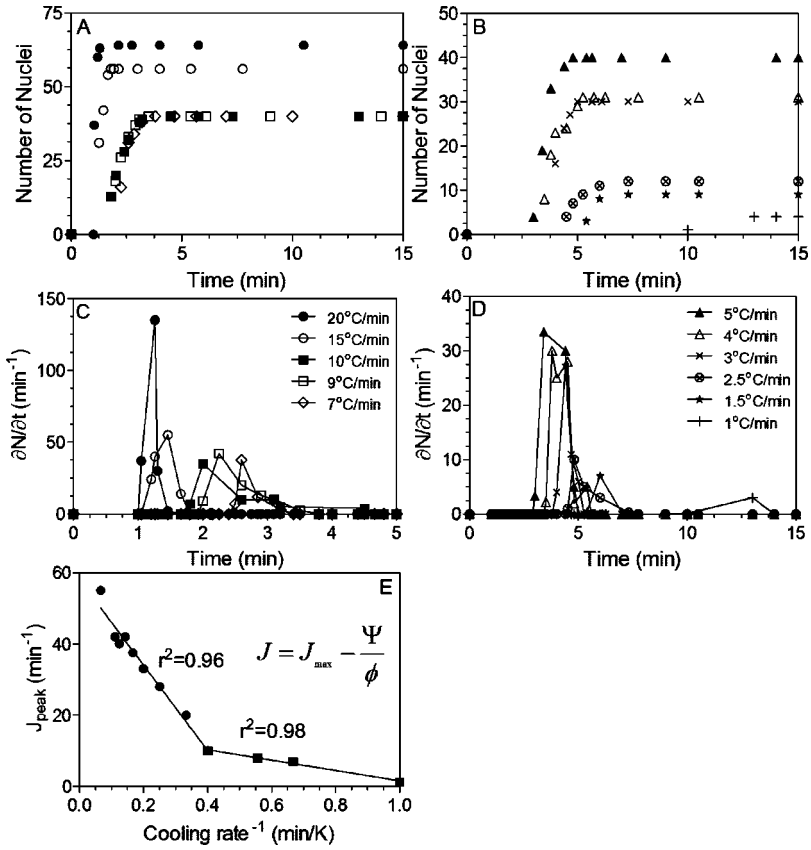


**Figure 2.** (A, B) Number of nuclei counted on bright-field micrographs as the sample was cooled nonisothermally, (C, D) the rate of nucleation determined by the change in the number of nuclei per unit time and (E) $J_{max}$, the maximum nucleation rate, which is a fitted parameter that is a function of cooling rate.

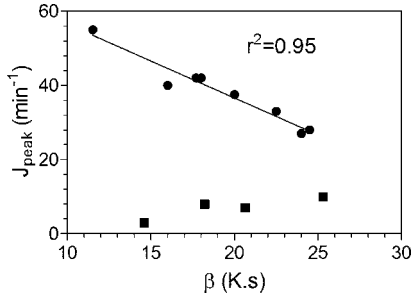


**Figure 3.** Variation of the nucleation rate ($J$) verses the supercooling-time exposure ($\beta$) for 2% 12HSA−canola oil.

which is similar to the melting temperature of 12HSA−canola oil (Figure 4D, dashed line) and it is evident that there is hydrogen bonding between carbonyl groups at temperatures starting at 65 °C, well above the crystallization temperature. The integral of the hydroxyl peak was taken to see if there was a change in the amount of hydrogen bonding as a function of time and temperature (Figure 4C). It was evident that hydrogen bonding was increase as a function of cooling and an increase in the amount of hydroxyl interactions increased above the crystallization temperature. It is interesting to note that there seems to be a large amount of hydrogen bonding at elevated temperatures, perhaps the reduction at 65 °C is due to a release of energy during the crystallization process. FTIR indicates that there is signification hydrogen bonding between both the hydroxyl and carbonyl groups in the melt supporting the microscopic phase separation argument.

**Crystal Growth Kinetics.** To quantify the rate of crystalline fiber growth, we manually measured the length of the fibers on each micrograph (Figure 1). A modified Avrami equation was then fitted to the data in order to characterize the crystal growth kinetics in terms of rate of growth.[18] The modified Avrami model had the form

$$Y = Y_{max}(1 - e^{-k_{app}(x - x_o)^n}) \quad (6)$$

where $Y$ is the fiber length, $Y_{max}$ the maximum length of the fiber, $k_{app}$ the apparent rate constant of fiber elongation, $x_o$ is the induction time, and $n$ is the dimensionality of growth. The Avrami model was originally developed for isothermal conditions. Here, however, we used it to characterize nonisothermal growth kinetics. This is strictly not correct; however, we found an excellent fit to the data and decided to use it nevertheless as a characterization tool. This is the reason we use the terminology "apparent" to refer to the rate constant of fiber growth. The Avrami index, $n$, was fixed as a constant ($n = 2$) because we observed sporadic one-dimensional growth as observed in the micrographs (panels A and B in Figure 1). Upon fitting the model to the experimental data (Figure 5), the constants for $Y_{max}$, $x_o$, and $k_{app}$ were determined (Figure 5C−E). The calculated $Y_{max}$ corresponded very well with the experimental data confirming that this model was a good tool to characterize nonisothermal self-assembled fibrillar network (SAFiN) growth of 12HSA. Furthermore, we observed that there was a drastic difference in the final length of the fibers depending on the cooling rate. Cooling rates above 5 °C/min lead to the formation of shorter fibers because of a greater number of nuclei formed initially, and thus less crystal growth took place. The calculated induction times did not correspond as well to the first signs of nuclei on the micrographs. The onset of crystal growth was taken as the first visible sign of crystalline mass using brightfield microscopy; however, this value was much higher than the one predicted using the Avrami model. This could be explained by

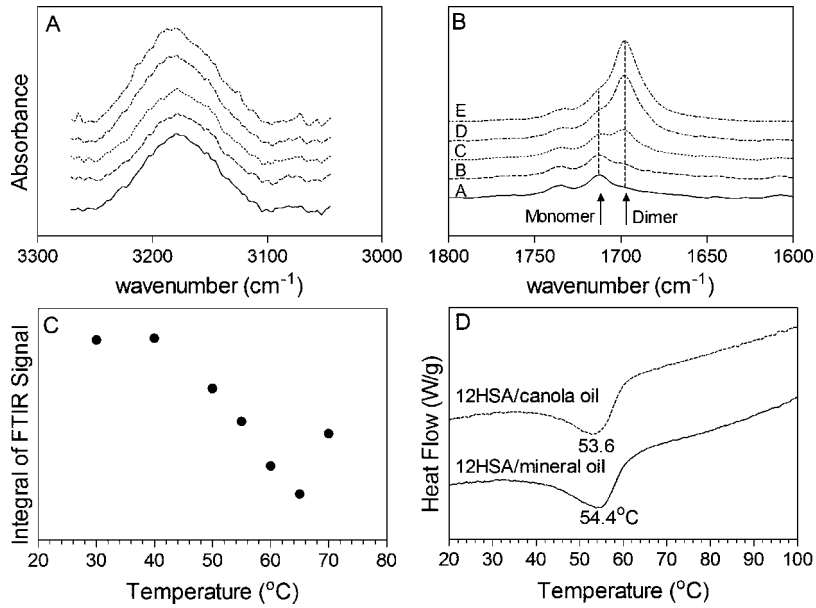


**Figure 4.** (A, B) FTIR spectrum of 2% 12HSA−mineral oil cooled at 1 °C/min and held for 15 min at each temperature before the scan. (C) The area under the hydroxyl portion was taken to see the change in the amount of hydrogen bonding associated with the 12-hydroxyl group. (D) The melting profiles measured using DSC were measured at 1 °C/min for both 2% 12HSA−canola oil and 2% 12HSA−mineral oil.

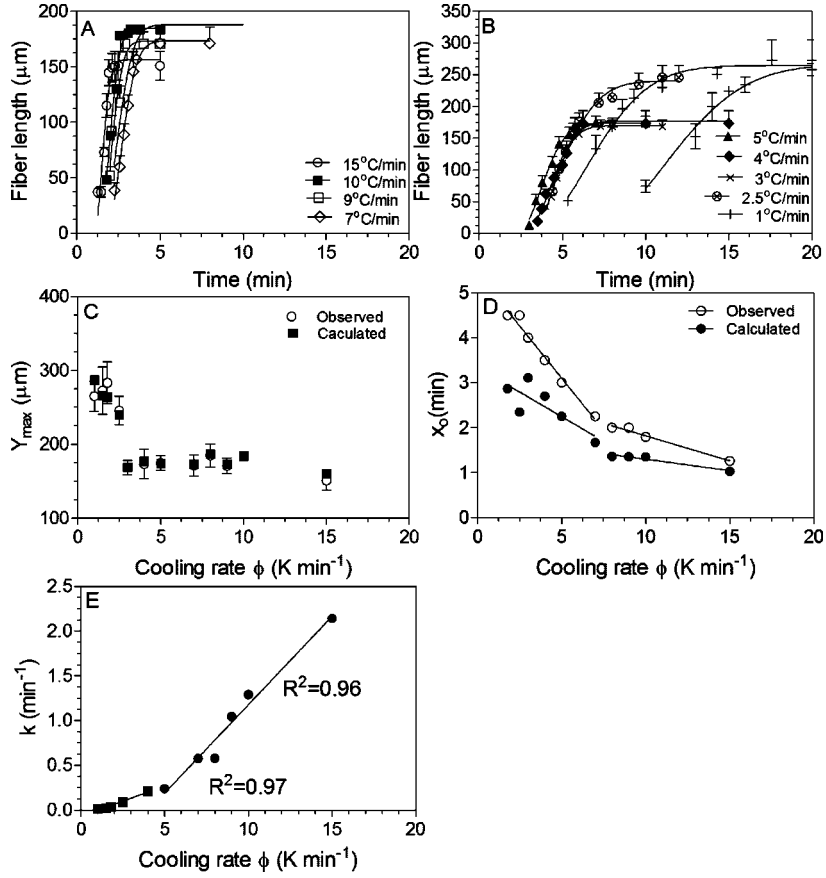


**Figure 5.** (A, B) Fiber length as a function of time/temperature supercooling trajectory measured using image J on bright-field micrograph and the Avarmi exponents, (C) $Y_{max}$, maximum fiber length, (D) $x_o$, induction time, and (E) $K$, rate constant.

a lack of sensitivity of the microscopy technique. Nevertheless the same general trends were followed for both the nuclei observed on the micrographs and calculated predicted values.

Change in the Avrami constant for fiber elongation as a function of cooling rate followed the same trends as that of the peak nucleation rates (Figure 5E). It appears that there are two different mechanisms which are influencing the rate of nucleation and crystal growth. The time-dependent thermodynamic driving force at high cooling rates leads to a greater rates of both crystal growth and nucleation. This regime of nucleation would be similar to that described by Wang, Lui, Xiong, and Li's in relation to their proposed nucleation-growth-noncrystallographic branching growth mechanism.[13] They suggested that an increase in the supersaturation would lead to a decrease in the crystallographic mismatch barrier, which in turn would increase fiber tip branching probability and lead to a more highly

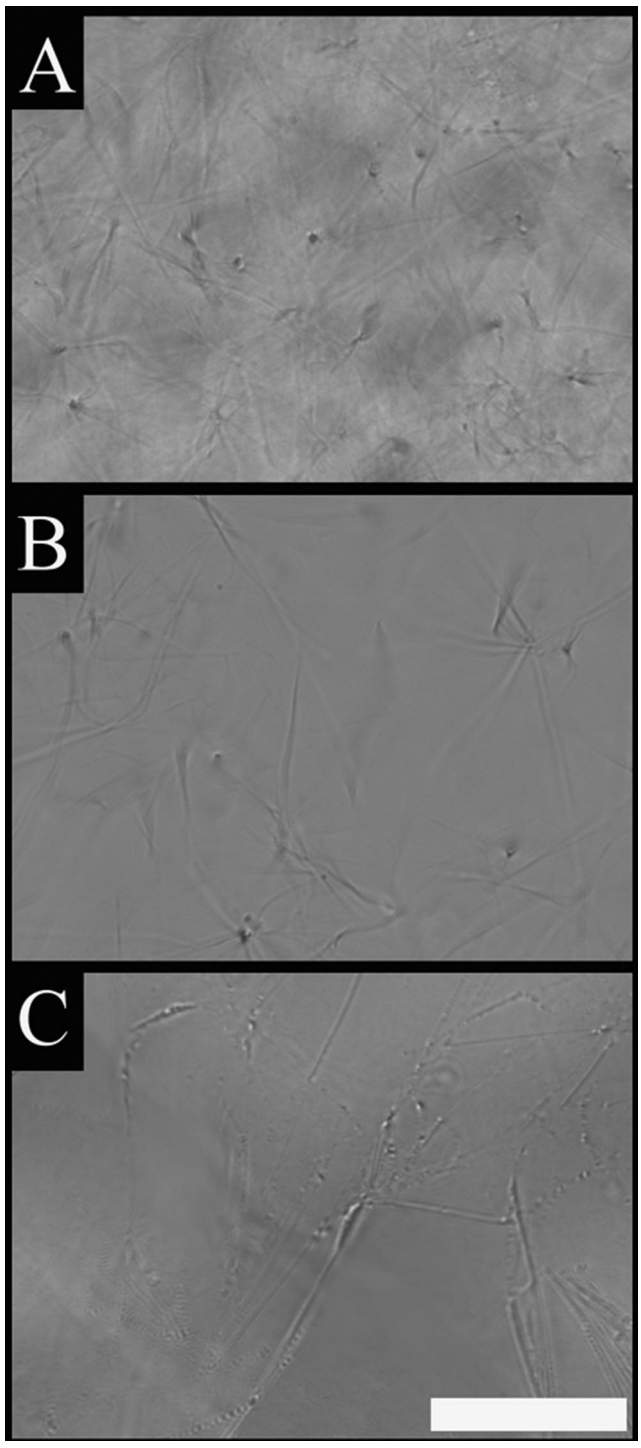


**Figure 6.** 2% 12HSA−canola oil cooled at (A) 10 and (B) 1 °C/min, and (C) 2%HSA/mineral oil cooled at 1 °C/min. Magnification bar = 100 $\mu$m.

branched network.[13] The junction zones and branching between polymer-like SAFIN strands are responsible for the rigidity of the networks that form.[13] If we compare our micrographs of a sample cooled at a rate faster than 5 °C/min and slower than this we can see significant differences in the morphology of the network (Figure 6). Slow cooling rates lead to systems with fewer nuclei with very little branching. These fibers grow to lengths of several hundred microns with little to no branching. This type of system would not effectively entrain liquid oil and would exhibit syneresis very rapidly.[4] Conversely, in the regime where nucleation is a strong function of the supercooling-time exposure, significantly more nucleation takes place, leading to the creation of a highly branched network which can bind oil more effectively[4] Therefore, in order to engineer the oil binding capacity and hardness/elasticity of an organogel, external fields could be modified in order to achieve a specific energy of nucleation. This in turn would not only dictate the amount of nuclei present, but would also define the degree of branching and fiber length of the SAFIN network. Future work should define those critical ranges of nucleation behavior.

## Conclusions

The nonisothermal nucleation rate of a self-assembling fibrillar network of 12-hydroxystearic acid in canola oil was found to be inversely proportional to the undercooling-time exposure of the system which was accurately modeled using the modified Avarmi equation. Distinct regions above and below 5 °C/min were observed for both nucleation and fiber growth kinetics. The abrupt change in the rate of nucleation, crystal growth rate constant, and the degree of branching at this cooling rate are related to whether the nucleation and crystal growth processes are governed by mass transfer or thermodynamics. We provided significant evidence for the argument of microscopic phase separation using FTIR to monitor the hydrogen bonding of the hydroxyl and carboxyl groups in the melt. This argument explains the difference for SAFiN and TAG crystallization. Using the models developed and adapted in this work, we could accurately predict the fiber length, rate of nucleation, rate of crystal growth, induction time of nucleation, and the degree of branching of a 12HSA SAFIN.

## References

(1) Terech, P.; Weiss, R. G. *Chem. Rev.* **1997**, *97*, 3133.
(2) Giorgano, J.; Daleo, C.; Stacks, S. M. *Eur. J. Pharmacol.* **1998**, *354*, 1.
(3) Kantaria, S.; Rees, G. D.; Lawrence, M. J. *J. Controlled Release* **1999**, *60*, 355.
(4) Rogers, M. A.; Wright, A. J.; Marangoni, A. G. *Curr. Opin. Colloid Interface Sci.* **2008**, doi:10.1016/j.cocis.2008.02.004.
(5) Marangoni, A. G.; McGualey, S. E. *Cryst. Growth Des.* **2003**, *3*, 95.
(6) Terech, P.; Furman, I.; Weiss, R. G. *J. Phys. Chem.* **1995**, *99*, 9558.
(7) Suzuki, M.; Nakajima, Y.; Yumoto, M.; Kimura, M.; Shirai, H.; Hanabusa, K. *Langmuir* **2003**, *19*, 8622.
(8) Rogers, M. A.; Wright, A. J.; Marangoni, A. G. *J. Am. Oil Chem. Soc.* **2007**, *84*, 899.
(9) Huang, X.; Raghavan, S. R.; Terech, P.; Weiss, R. G. *J. Am. Chem. Soc.* **2006**, *128*, 15341.
(10) Li, J. L.; Liu, X. Y.; Strom, C. S.; Xiong, J. Y. *Adv. Mater.* **2006**, *18*, 2574.
(11) Tan, G.; John, V. T.; McPherson, G. L. *Langmuir* **2006**, *22*, 7416.
(12) Lui, X. Y.; Sawant, P. D. *Appl. Phys. Lett.* **2001**, *79*, 3518.
(13) Wang, R.; Lui, X.-Y.; Xiong, J.; Li, J. *J. Phys. Chem. B* **2006**, *110*, 7275.
(14) Marangoni, A. G.; Tang, D.; Singh, A. P. *Chem. Phys. Lett.* **2006**, *419*, 259.
(15) Marangoni, A. G.; Tang, D.; Singh, A. P. *Chem. Phys. Lett.* **2005**, *419*, 259.
(16) Weiss, R. G.; Terech, P. In *Molecular Gels Materials with Self-Assembled Fibrillar Networks*; Weiss, R. G., Terech, P., Eds.; Springer: New York, pp 1−16.
(17) Huang, X.; Terech, P.; Raghavan, S. R.; Weiss, R. G. *J. Am. Chem. Soc.* **2005**, *127*, 4336.
(18) Rousset, P. In *Physical Properties of Lipids*; Marangoni, A. G., Narine, S. S., Eds.; Marcel Dekker: New York, 2002.

CG8008927